Anisotropic magnetoresistance of thin $La_{0.7}Ca_{0.3}MnO_3$ films

1998 J. Phys.: Condens. Matter 10 2727

(http://iopscience.iop.org/0953-8984/10/12/012)

J. Phys.: Condens. Matter **10** (1998) 2727–2737. Printed in the UK PII: S0953-8984(98)89798-1

Anisotropic magnetoresistance of thin $La_{0.7}Ca_{0.3}MnO_3$ films

M Ziese and S P Sena

Department of Physics, University of Sheffield, Sheffield S3 7RH, UK

Received 4 December 1997

Abstract. The low-field magnetoresistance of $La_{0.7}Ca_{0.3}MnO_3$ films deposited on different substrates has been measured. Whereas post-annealed films on $SrTiO_3$ and $LaAlO_3$ exhibit a clear anisotropic magnetoresistance (AMR), the low-field magnetoresistance of as-deposited films on $LaAlO_3$ and Si is dominated by grain-boundary magnetoresistance. At low temperatures the anisotropic magnetoresistance is temperature independent with a value of about $-0.2 \pm 0.1\%$. A simple atomic d-state model can explain the sign of the anisotropic magnetoresistance.

1. Introduction

The resistivity of manganite thin films exhibits a strong dependence on the magnetization. In applied fields of several teslas and near the Curie temperature a colossal magnetoresistive (CMR) effect is seen [1]. However, a direct application of this galvanomagnetic effect is precluded by the high fields needed to induce it. Therefore recent research activity has concentrated on the low-field regime [2–6].

In this work we show that two mechanisms contribute to the low-field magnetoresistance, i.e., anisotropic magnetoresistance (AMR) and grain-boundary resistance. In contrast to the results of previous studies of anisotropic magnetoresistance in the manganites [7] we find a clear AMR signal in post-annealed $La_{0.7}Ca_{0.3}MnO_3$ films on $SrTiO_3$ and $LaAlO_3$. The AMR at low temperatures is found to be small, i.e., about -0.2%, whereas the grain-boundary magnetoresistance can reach appreciable values of -5% at low temperatures in polycrystalline films. However, an AMR maximum of up to -2% in moderate fields is found in epitaxial films near the Curie temperature. The existence of anisotropic magnetoresistance in the manganites implies some 'fine structure' in the d bands that goes beyond the basic double-exchange model [8, 9].

2. Film preparation and experimental details

$La_{0.7}Ca_{0.3}MnO_3$ films were grown by laser ablation (XeCl, 308 nm) from a stoichiometric target at an oxygen partial pressure of 100 mTorr and a substrate temperature of about 700 °C. High-quality epitaxial films were produced by this route on $LaAlO_3$(001) and $SrTiO_3$(001) substrates with an as-deposited Curie temperature, T_C, of about 230 K and a resistivity maximum in zero field, T_R, of 235 K. A post-annealing treatment for 2 h at 950 °C in flowing oxygen yields films with a T_C of about 275 K and a T_R of 290 K. The deposition on Si(001) leads to the formation of polycrystalline films. These films still have Curie temperatures above 200 K, but the metal/insulator transition is broad and the overall

0953-8984/98/122727+11$19.50

resistivity is roughly three orders of magnitude higher than in epitaxial films. An annealing treatment at 950 °C in flowing oxygen does not lead to an improvement of the film qualities of films on Si(001).

In this work we report extensive resistivity and magnetization measurements on (a) an annealed film on $SrTiO_3$ (LC229SR), (b) an as-deposited film on $LaAlO_3$ (LC156LA) and (c) an as-deposited film on Si (LC259SI).

Resistivity measurements were performed using a four-point technique. A constant current between 10 μA and 1 mA was supplied by a homemade constant-current source and the voltage was measured with a Keithley model 182 nanovoltmeter; current reversal ensured the elimination of thermal voltages. Contacts were made with silver paint. For measurements on film LC229SR a van der Pauw [10] configuration was used, whereas four in-line contacts were used to measure the resistance of the other films. The resistance of film LC229SR was checked with an in-line contact configuration and essentially the same results were obtained as in the van der Pauw configuration. The current was always applied along the same current path directed along (100).

Magnetization measurements were performed with a SQUID magnetometer (Quantum Design, MPMS-5).

3. The model

The anisotropic magnetoresistance is commonly defined as [11]

$$\mathrm{AMR} = \frac{\rho_\parallel - \rho_\perp}{\rho_{\mathrm{ave}}}. \tag{1}$$

$\rho_\parallel$ and $\rho_\perp$ denote the longitudinal (magnetic field parallel to the current) and transverse (magnetic field perpendicular to the current) resistivities, respectively. The resistivity should be extrapolated to zero induction, $B = 0$, and $\rho_{\mathrm{ave}} = (1/3)\rho_\parallel + (2/3)\rho_\perp$.

Detailed investigations of the resistivity of nickel alloys have shown that the anisotropic magnetoresistance of those alloys can be understood within a two-current model incorporating the spin–orbit interaction [12, 13]. In this model majority (spin-up) and minority (spin-down) electrons carry the electric current in parallel. The resistivity in each channel consists of two contributions, i.e., s-electron scattering into s and into d states. In nickel alloys the resistivity due to s–d scattering dominates. The anisotropic magnetoresistance can be estimated within a simple atomic state model.

According to the double-exchange model the electric current in the manganites is carried by d electrons hopping between neighbouring manganese sites [8, 9]. The application of a model based on s–d scattering means that the hopping manganese d electron is approximated by a plane wave. Although a description by a tight-binding Bloch wave seems more appropriate, we use the plane-wave model here as a starting point for understanding the magnitude and sign of the observed anisotropic magnetoresistance.

The derivation of the anisotropic magnetoresistance presented here follows the reasoning of Malozemoff [14]. The starting point is a Hamiltonian that includes a crystal-field splitting Δ_{CF} and an exchange-coupling energy H_{ex}. The spin–orbit interaction H_{so} is introduced as a small perturbation with

$$H_{\mathrm{so}} = A\left[L_z S_z + \frac{1}{2}(L_+ S_- + L_- S_+)\right]. \tag{2}$$

The ten d-state wave functions for both spin directions are calculated to second order in the spin–orbit coupling. Since the Fermi energy lies in the manganite $e_{g\uparrow}$ band [1], we

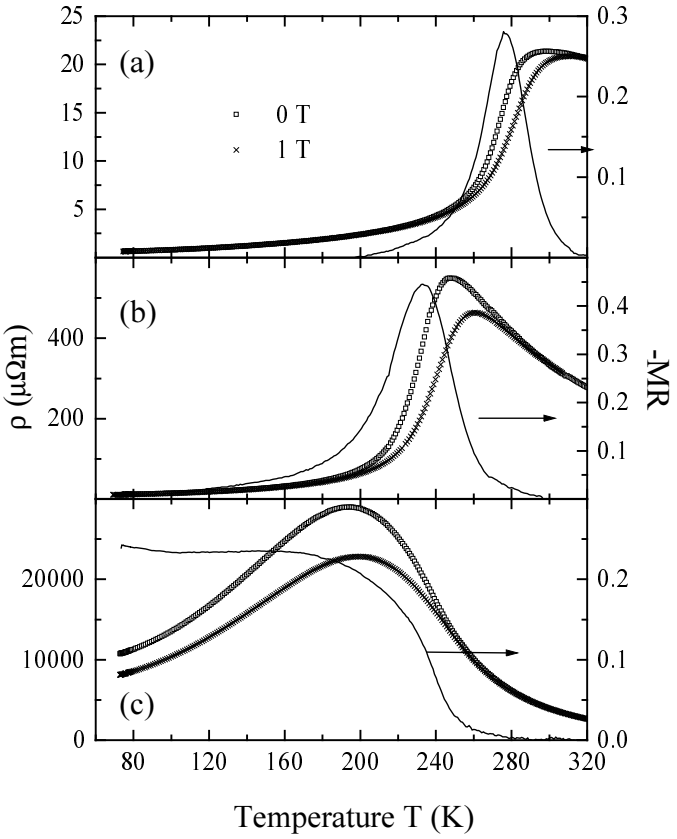

Figure 1. The resistivity in zero field and 1 T applied parallel to the film (symbols) and the magnetoresistance ratio MR at 1 T (solid lines) of different $La_{0.7}Ca_{0.3}MnO_3$ films: (a) a post-annealed film on $SrTiO_3$ (LC229SR), (b) an as-deposited film on $LaAlO_3$ (LC156LA) and (c) an as-deposited film on Si (LC259SI).

concentrate on the $e_{g\uparrow}$ states in the following. The perturbed wave functions ψ are to second order

$$\psi^{(1)}_{e_{g\uparrow}} = \left(1 - \delta^2 - \frac{1}{2}\epsilon_-^2\right)\phi_{x^2-y^2\uparrow} - \frac{1}{\sqrt{2}}\left(\epsilon_- - \frac{\epsilon_-^2\delta}{\epsilon} + \frac{1}{2}\epsilon_-^2\right)\phi_{-1\downarrow} + \mathrm{i}\left(\delta + \frac{1}{2}\epsilon_-\delta\right)\phi_{xy\uparrow} \tag{3a}$$

$$\psi^{(2)}_{e_{g\uparrow}} = \left(1 - \frac{3}{2}\epsilon_-^2\right)\phi_{3z^2-r^2\uparrow} - \sqrt{6}\left(\frac{1}{2}\epsilon_- + \epsilon_-^2\right)\phi_{+1\downarrow} \tag{3b}$$

with energies

$$E_1 = -\frac{1}{2}H_{\mathrm{ex}} + \frac{1}{2}H_{\mathrm{ex}}\left(\frac{\epsilon}{\delta} + 2\epsilon\delta - \epsilon\epsilon_-\right) \tag{4a}$$

$$E_2 = -\frac{1}{2}H_{\mathrm{ex}} + \frac{1}{2}H_{\mathrm{ex}}\left(\frac{\epsilon}{\delta} - 3\epsilon\epsilon_-\right). \tag{4b}$$

The following abbreviations are used: $\epsilon = A/H_{\mathrm{ex}}$, $\epsilon_- = A/(H_{\mathrm{ex}} - \Delta_{\mathrm{CF}})$ and $\delta = A/\Delta_{\mathrm{CF}}$. $\phi_{x^2-y^2\uparrow}$, $\phi_{3z^2-r^2\uparrow}$, $\phi_{xy\uparrow}$, $\phi_{-1\downarrow}$ and $\phi_{+1\downarrow}$ denote the unperturbed atomic d states.

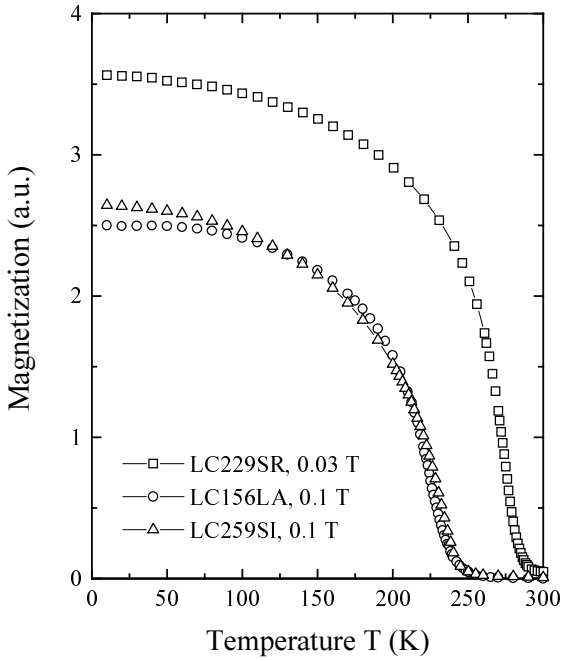

Figure 2. Magnetization at constant applied field as a function of temperature for the three films shown in figure 1.

The resistivity is estimated from the scattering of a plane wave incident parallel or perpendicular to the magnetization. Taking only $e_{g\uparrow}$ states and incoming spin-up electrons into account we obtain [15]

$$\frac{\rho_{\parallel} - \rho_{\perp}}{\rho_{\text{ave}}} = -\frac{3}{2}\left[\frac{A^2}{(H_{\text{ex}} - \Delta_{\text{CF}})^2} - \frac{A^2}{\Delta_{\text{CF}}^2}\right]. \tag{5}$$

The anisotropy arises due to the $L_z S_z$-term in the spin–orbit coupling, i.e., it is an intraband effect.

4. Results

Figure 1 shows the resistivity of (a) the annealed $La_{0.7}Ca_{0.3}MnO_3$ film on $SrTiO_3$ (LC229SR), (b) the as-deposited film on $LaAlO_3$ (LC156LA) and (c) the as-deposited film on Si (LC259SI) as a function of temperature in zero field and with a magnetic field of 1 T applied parallel to the film. The resistivities ρ and the magnetoresistance at 1 T, MR, given by

$$\text{MR} = [\rho(1\,\text{T}) - \rho_0]/\rho_0 \tag{6}$$

are in agreement with published values [1]. ρ_0 denotes the zero-field resistivity. In figure 2 the magnetization of the samples is shown as a function of temperature. The Curie temperatures estimated from the minimum in the magnetization derivative are 275.2 K for the post-annealed film LC229SR, and 224.6 K (LC156LA) and 230.5 K (LC259SI) for the as-deposited films. The magnetizations of the as-deposited samples on $LaAlO_3$ and Si are nearly identical, whereas the resistive behaviours are markedly different, thus indicating the

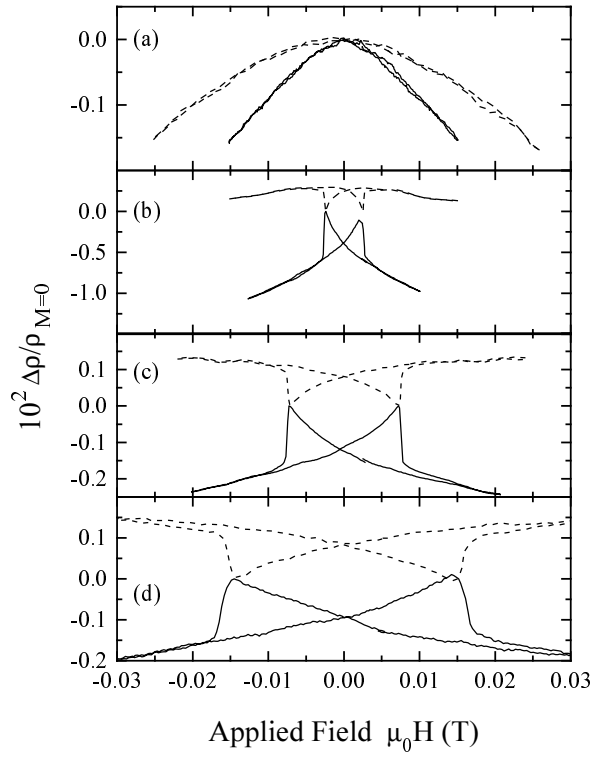

Figure 3. The longitudinal (solid lines) and transverse (dashed lines) magnetoresistance of the post-annealed sample on $SrTiO_3$, LC229SR, at (a) 285.3 K, (b) 264.1 K, (c) 201.3 K and (d) 96.1 K.

importance of grain-boundary effects on the resistivity of the sample on Si [3]. The high Curie temperatures of the as-deposited as well as the annealed films on $SrTiO_3$ and $LaAlO_3$ and the fact that the temperature of maximal resistivity is close to T_C prove the high quality of our samples.

The low-field magnetoresistance has been measured at constant temperatures T such that 90 K $< T <$ 310 K in magnetic fields applied parallel and perpendicular to the electric current. The magnetic field was always oriented parallel to the film. Figures 3–5 show the normalized resistivities

$$\Delta\rho_{\parallel}/\rho_{M=0} = \rho_{\parallel}/\rho_{M=0} - 1 \tag{7}$$

and

$$\Delta\rho_{\perp}/\rho_{M=0} = \rho_{\perp}/\rho_{M=0} - 1 \tag{8}$$

as a function of magnetic field for the three samples investigated at some selected temperatures. The resistivity is shown in comparison to the magnetization measured in the film plane in figure 6. The extrema in the resistivity are seen to occur at zero magnetization, i.e., at the coercive fields. At these fields an appreciable fraction of domains are oriented parallel (transverse geometry) or perpendicular (longitudinal geometry) with respect to the current, thus yielding minima and maxima in the resistivity, respectively.

The post-annealed sample LC229SR shows a resistivity behaviour reminiscent of those of cobalt and nickel—see e.g. reference [16]—i.e., well below the Curie temperature, $\Delta\rho_{\parallel}$

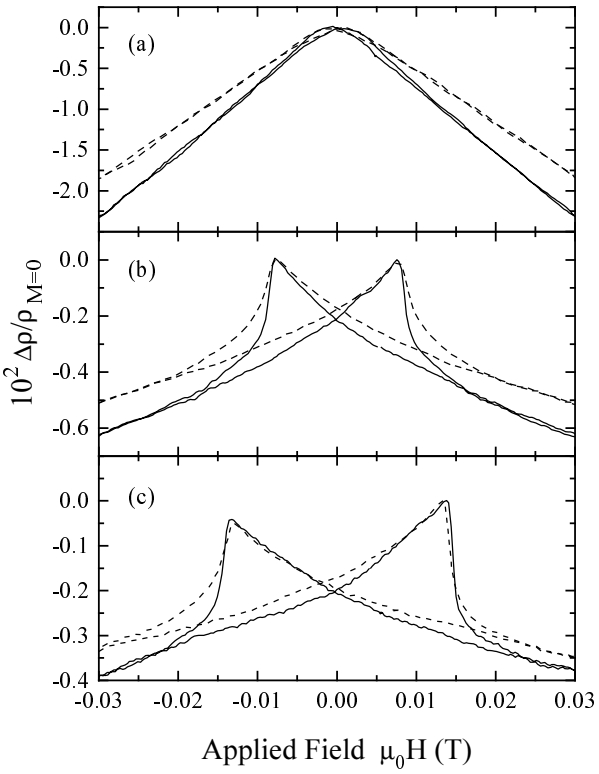

Figure 4. The longitudinal (solid lines) and transverse (dashed lines) magnetoresistance of the as-deposited sample on $LaAlO_3$, LC156LA, at (a) 232.2 K, (b) 158.8 K and (c) 95.7 K.

and $\Delta\rho_\perp$ have different signs. The longitudinal resistivity reaches a maximum at the coercive field, whereas the transverse resistivity shows a relative minimum; this finding is opposite to the situation in cobalt and nickel which at the coercive field show minima in the longitudinal and maxima in the transverse resistivity. The same resistivity behaviour is found for a post-annealed film on $LaAlO_3$ at 96 K.

The as-deposited films on $LaAlO_3$ (LC156LA) and Si (LC259SI), however, show a completely different behaviour. For both films the longitudinal as well as the transverse resistivity exhibit maxima at the coercive field and largely the same functional dependence on magnetic field. Only at higher fields does a small difference emerge: the transverse resistivity at high fields is always larger than the longitudinal resistivity. The low-field magnetoresistance effect is largest in the polycrystalline $La_{0.7}Ca_{0.3}MnO_3$ film on Si and much smaller in the epitaxial film on $SrTiO_3$.

To investigate the dependence of the low-field magnetoresistance on the microstructure, we proceed as follows. We determine the drop in the longitudinal resistivity at the coercive field at 96 K:

$$\frac{\Delta\rho_\parallel}{\rho_0}(H_c). \tag{9}$$

In figure 6 $\Delta\rho_\parallel/\rho_{M=0}(H_c)$ is indicated; this is converted into $\Delta\rho_\parallel/\rho_0(H_c)$. This quantity gives a rough measure of the low-field magnetoresistance. Since the transport properties are strongly dependent on the microstructure [3] we use the zero-field resistivity ρ_0 at

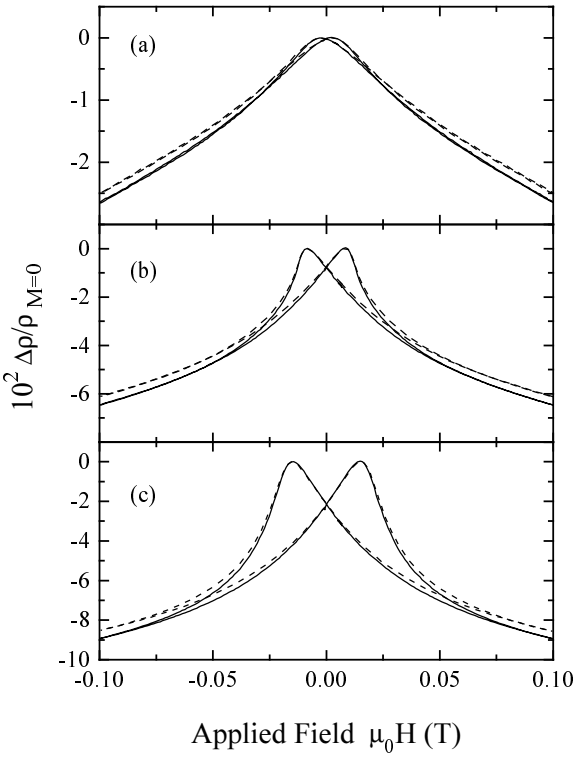

Figure 5. The longitudinal (solid lines) and transverse (dashed lines) magnetoresistance of the as-deposited sample on Si, LC259SI, at (a) 211.3 K, (b) 158.9 K and (c) 96.4 K.

96 K as an indicator of the sample quality. Figure 7(a) shows results for a variety of $La_{0.7}Ca_{0.3}MnO_3$ films on $LaAlO_3$, $SrTiO_3$, Si and quartz substrates. The low-field magnetoresistance increases with the zero-field resistivity. We find (see the solid line in figure 7)

$$\frac{\Delta\rho_{\parallel}}{\rho_0}(H_c) \propto \sqrt{\rho_0}. \tag{10}$$

In figure 7(b) the coercive fields of the samples investigated are shown. The coercive fields are surprisingly constant over the wide range of film qualities investigated here. This proves that $\Delta\rho_{\parallel}/\rho_0(H_c)$ is determined not by the coercivity but by the transport properties.

In figure 7(a) the low-field magnetoresistance of single grain boundaries as determined in [17] and [18] is shown by solid triangles. The resistivity of a single grain boundary was estimated from the areal resistivity by assuming a grain-boundary thickness of 1 nm [18]. Our results on different films extrapolate nicely to the results for single grain boundaries. Therefore we conclude that the low-field magnetoresistance mainly has two contributions, i.e., a contribution from the anisotropic magnetoresistance and a second contribution from the grain-boundary magnetoresistance. The grain-boundary magnetoresistance is found to be much larger than the anisotropic magnetoresistance. Since the longitudinal and transverse magnetoresistances of the post-annealed sample are not fully symmetric with respect to the field axis—see figure 3—we cannot exclude the possibility of a small contribution from grain-boundary scattering in this sample.

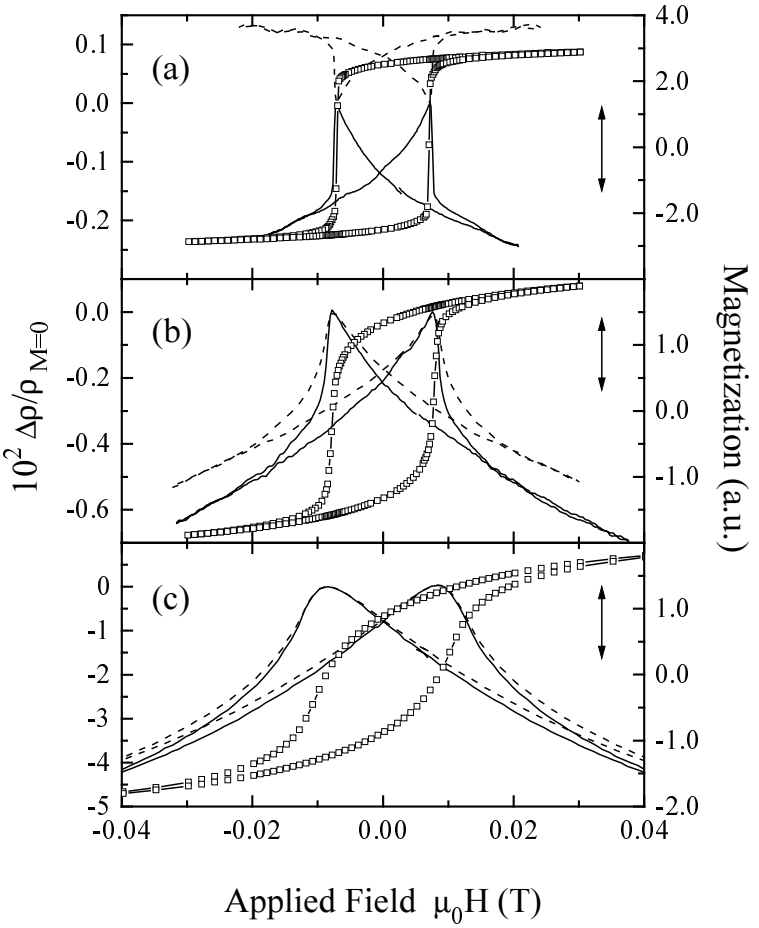

Figure 6. The longitudinal (solid lines) and transverse (dashed lines) magnetoresistance (left-hand axis) and magnetization (□) (right-hand axis) of (a) LC229SR at 201.3 K, (b) LC156LA at 158.8 K and (c) LC259SI at 158.9 K. The arrows indicate the definition of $\Delta\rho_{\parallel}/\rho_{M=0}(H_c)$.

In the following we concentrate on the anisotropic magnetoresistance. Figure 8 shows the anisotropic magnetoresistance AMR $= (\rho_{\parallel} - \rho_{\perp})/\rho_{M=0}$ for the three samples investigated as a function of temperature at different magnetic fields. Since the grain-boundary resistance is isotropic, it cancels in the calculation of the AMR. It was not possible to extrapolate the resistivity to $B = 0$. Therefore we use $\rho_{M=0}$ instead of ρ_{ave} as a normalizing factor. For sample LC229SR this procedure introduces a negligible error, since the low-field magnetoresistance is rather small. Measurements of the longitudinal and transverse magnetoresistance of a post-annealed $La_{0.7}Ca_{0.3}MnO_3$ film on $LaAlO_3$ yield AMR $= -0.15\%$ at 96 K and 0.03 T. This value was checked by measurements of the angular dependence of the resistivity and was found to be consistent.

For all of the samples investigated, at low temperatures we find a nearly temperature-independent AMR value of about -0.2%. The epitaxial films show an AMR maximum close to T_C—see figures 8(a) and 8(b)—that follows the colossal magnetoresistance (CMR) maximum. This indicates that the AMR is caused by the same scattering processes as the CMR.

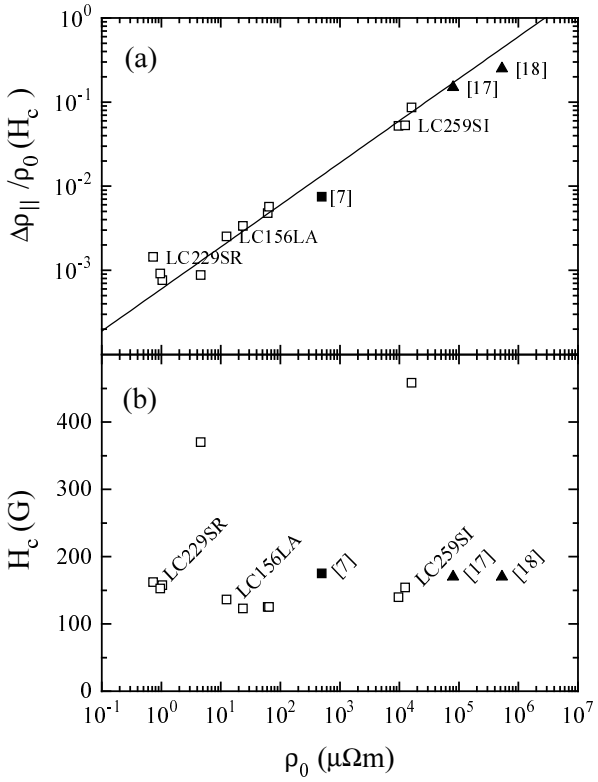

Figure 7. (a) Low-field magnetoresistance $\Delta\rho/\rho_0(H_c)$ and (b) coercive fields H_c as functions of the zero-field resistivity ρ_0 at 96 K. Open symbols: this work; solid square: epitaxial film (O'Donnell *et al* [7]); solid triangles: individual grain boundary (Mathur *et al* [17] and Steenbeck *et al* [18]).

5. Discussion

From the measurement of three $La_{0.7}Ca_{0.3}MnO_3$ films we consistently obtained a constant low-temperature value of the anisotropic magnetoresistance AMR $= -0.2 \pm 0.1\%$. We believe that this value is intrinsic since we did not find a systematic dependence on the microstructure. Moreover, the post-annealed film on $SrTiO_3$ appears to be of excellent quality, i.e., contains only very few grain boundaries. This value is in agreement with the value reported by Li *et al* [4] for an epitaxial $La_{0.67}Sr_{0.33}MnO_3$ film on $SrTiO_3$ at 4.2 K.

In section 2 a simple atomic model for the magnetoresistance was introduced. In the manganites the crystal-field splitting is $\Delta_{CF} \simeq 1.5$ eV and the exchange splitting is $H_{ex} \simeq 2.0$ eV [1]. The atomic value for the spin–orbit coupling of first-series transition elements is $A = 0.04$ eV [13]. From these numbers we obtain an anisotropic magnetoresistance AMR $= -0.85\%$.

There are two features to note: (1) the model predicts the correct sign and (2) the predicted magnitude is reasonable. The prediction of the correct sign indicates that the assumed bandstructure, i.e., a Fermi energy completely lying in the $e_{g\uparrow}$ band, is correct. The effect is due to the L_zS_z-term in the spin–orbit interaction that leads to an energy splitting of the $e_{g\uparrow}$ states, i.e., it is an intra-band effect. Considering the simplicity of the model, the agreement between the measured and calculated AMR is surprising. We tried to

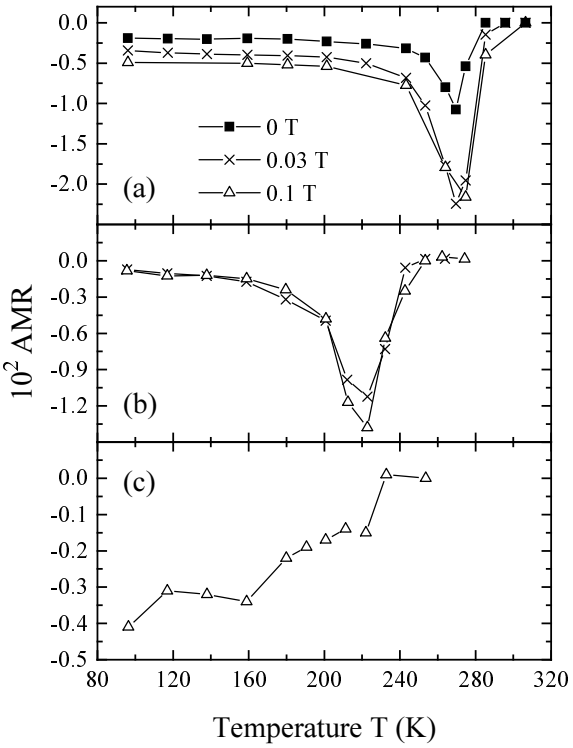

Figure 8. The anisotropic magnetoresistance AMR as a function of temperature of (a) the post-annealed sample LC229SR, (b) the as-deposited sample LC156LA and (c) the as-deposited sample LC259SI.

improve the model by calculating the resistivity of a tight-binding Bloch wave scattered into atomic d states. Unfortunately the result involves an unknown scattering matrix element as an additional parameter and this is therefore not helpful for the interpretation of the experimental data.

6. Conclusions

In this work we investigated the low-field magnetoresistance of $La_{0.7}Ca_{0.3}MnO_3$ films grown under different conditions on various substrates. Two processes contribute to the low-field magnetoresistance, i.e., the anisotropic magnetoresistance (AMR) and the grain-boundary magnetoresistance. Whereas the grain-boundary resistance strongly depends on the microstructure, the AMR is an intrinsic property. At low temperatures the AMR is temperature independent with AMR $= -0.2 \pm 0.1\%$. A simple atomic model for the scattering of plane waves into d states yields a value AMR $= -0.85\%$ in surprisingly good agreement with the data.

Since the low-field magnetoresistance is strongly microstructure dependent, it might be a good indicator of sample quality. The observation of a positive transverse magnetoresistance at temperatures far below the Curie temperature proves the excellent quality of our post-annealed $La_{0.7}Ca_{0.3}MnO_3$ films on $SrTiO_3$ and $LaAlO_3$.

Acknowledgments

This work was supported by the European Union TMR 'OXSEN' network. We acknowledge useful discussions with G A Gehring, H J Blythe and M R J Gibbs.

References

[1] Coey J M D, Viret M and von Molnar S 1998 *Adv. Phys.* at press
[2] Gupta A, Gong G Q, Xiao G, Duncombe P R, Lecouer P, Trouilloud P, Wang Y Y, Dravid V P and Sun J Z 1996 *Phys. Rev.* B **54** R15 629
[3] Hwang H Y, Cheong S-W, Ong N P and Batlogg B 1996 *Phys. Rev. Lett.* **77** 2041
[4] Li X W, Gupta A, Xiao G and Gong G Q 1997 *Appl. Phys. Lett.* **71** 1124
[5] Gibbs M R J, Ziese M, Gehring G A, Blythe H J, Coombes D J, Sena S P and Shearwood C 1998 *Phil. Trans. R. Soc.* at press
[6] Ziese M, Sena S P, Shearwood C, Blythe H J, Gibbs M R J and Gehring G A 1998 *Phys. Rev.* B **57** 2963
[7] O'Donnell J, Onellion M, Rzchowski M S, Eckstein J N and Bozovic I 1997 *Phys. Rev.* B **55** 5873
Eckstein J N, Bozovic I, O'Donnell J and Rzchowski M S 1996 *Appl. Phys. Lett.* **69** 1312
O'Donnell J, Onellion M, Rzchowski M S, Eckstein J N and Bozovic I 1997 *J. Appl. Phys.* **81** 4961
[8] Zener C 1951 *Phys. Rev.* **82** 403
[9] de Gennes P-G 1960 *Phys. Rev.* **118** 141
[10] van der Pauw L J 1959 *Philips Tech. Rev.* **20** 220
[11] Smit J 1951 *Physica* **16** 612
[12] Campbell I A, Fert A and Jaoul O 1970 *J. Phys. C: Solid State Phys.* **3** S95
[13] Jaoul O, Campbell I A and Fert A 1977 *J. Magn. Magn. Mater.* **5** 23
[14] Malozemoff A P 1986 *Phys. Rev.* B **34** 1853
[15] Note that the AMR derived in equation (5) is twice the value derived by Malozemoff. This is due to the fact that we only consider the $e_{g\uparrow}$ states in the calculation of the total resistivity.
[16] Viret M, Vignoles D, Cole D, Coey J M D, Allen W, Daniel D S and Gregg J F 1996 *Phys. Rev.* B **53** 8464
[17] Mathur N D, Burnell G, Isaac S P, Jackson T J, Teo B S, MacManus-Driscoll J L, Cohen L F, Evetts J E and Blamire M G 1997 *Nature* **387** 266
[18] Steenbeck K, Eick T, Kirsch K, O'Donnell K and Steinbeiß E 1997 *Appl. Phys. Lett.* **71** 968